Strongly Interacting Bosons in a Two-Dimensional Quasicrystal Lattice

Ronan Gautier, Hepeng Yao, and Laurent Sanchez-Palencia
CPHT, CNRS, Ecole Polytechnique, IP Paris, F-91128 Palaiseau, France

(Received 15 October 2020; accepted 16 February 2021; published 15 March 2021)

Quasicrystals exhibit exotic properties inherited from the self-similarity of their long-range ordered, yet aperiodic, structure. The recent realization of optical quasicrystal lattices paves the way to the study of correlated Bose fluids in such structures, but the regime of strong interactions remains largely unexplored, both theoretically and experimentally. Here, we determine the quantum phase diagram of two-dimensional correlated bosons in an eightfold quasicrystal potential. Using large-scale quantum Monte Carlo calculations, we demonstrate a superfluid-to-Bose glass transition and determine the critical line. Moreover, we show that strong interactions stabilize Mott insulator phases, some of which have spontaneously broken eightfold symmetry. Our results are directly relevant to current generation experiments and, in particular, drive prospects to the observation of the still elusive Bose glass phase in two dimensions and exotic Mott phases.

DOI: 10.1103/PhysRevLett.126.110401

Quasicrystals are a fascinating state of matter, characterized by long-range, although nonperiodic, order. Such exotic structures may be realized by the continuous tiling of space using sets of irreducible unit cells arranged aperiodically [1,2] or as incommensurable projections of periodic lattices in higher dimensions [3]. Such structures spontaneously appear in the growth of certain alloys [4–6] or can be engineered in photonic [7–10] and ultracold-atom [11–13] systems. The hallmark of quasicrystalline order, i.e. sharp spots in reciprocal space with a rotation symmetry incompatible with discrete translation invariance, can then be characterized using Bragg [4,14] or matterwave [15,16] diffraction. Quasicrystals exhibit unique properties, inherited from structural self-similarity at all scales. It includes nontrivial topological order [17–21] and Anderson-like localization [22,23], as well as the fractal properties of wave functions [24,25], energy spectrums [8,26–29], and phase diagrams [30]. So far, quasicrystals have been extensively studied in regard to solid-state physics [4–6], superconductivity [31], twisted bilayer graphene [32,33], photonic structures [34–37], and ultracold quantum gases [15,16,23,30,38–52].

Quasiperiodic Bose fluids are particularly appealing due to the complex interplay of interactions, localization, and quasiperiodicity. Controlled quasicrystal potentials for atomic systems, free of defects and phonons, can be optically designed using laser fields arranged in various rotation symmetries [15,38,44]. Alternatively, quasicrystals can be engineered using long-range interactions, spin-orbit coupling, and cavity-mediated interactions [53–55]. Moreover interactions can be tuned in wide ranges [56–58], hence offering a unique playground. Ultracold atoms in one-dimensional (1D) quasiperiodic potentials have been extensively studied in the context of Anderson localization [23,39,40,52], Bose glasses (BGs) [30,39–43,46,48], and collective [45] and many-body [47,49,50] localization. In contrast, much less is known in higher dimensions. Recently, the emergence of quasiperiodic order [16] and localization of weakly interacting bosons [51] in a two-dimensional (2D) eightfold quasicrystal have been reported. The existence of a BG and the regime of strong interactions, however, remains largely unexplored. On the theoretical side, mean field phase diagrams have been found using inhomogeneous Gutzwiller-like ansatz on simplified quasiperiodic graphs [59–61]. Such approaches are, however, mean field in nature and ignore the emergence of strong correlations close to critical points, as well as a realistic connectivity of optical quasicrystals.

In this Letter, we study correlated 2D bosons in an eightfold rotationally symmetric quasicrystal potential. Using path integral Monte Carlo calculations, we find exact quantum phase diagrams, taking into account possibly strong interactions and the full quasicrystalline structure of the potential. For weak interactions, we find a superfluid (SF) and a BG phase determined by the competition of interactions and localization. The SF order parameter shows a clear critical behavior, from which we extract the critical line in the interaction-quasicrystal amplitude diagram. In contrast, the compressibility shows a smooth crossover that is consistent with the compressible character of both phases. For strong-enough interactions, Mott lobes open within the BG phase due to the competition of particle repulsion, localization, and tunneling. In most cases, the total filling is a multiple of 8, which is consistent with the eightfold rotation symmetry of the potential. In some cases, however, we find a multiply-degenerated ground state manifold characterized by spontaneously broken rotation symmetry. We attribute this

behavior to the suppression of double occupancy in pairs of nearby potential wells. Finally, we discuss experimental and theoretical prospects.

Model and single-particle properties.—We consider a 2D gas of N interacting bosons of mass m in a quasicrystal potential $V(\boldsymbol{r})$. It is governed by the Hamiltonian

$$\hat{H} = \sum_j \left[-\frac{\hbar^2}{2m}\nabla_j^2 + V(\hat{\boldsymbol{r}}_j) \right] + \sum_{j<k} U(\hat{\boldsymbol{r}}_j - \hat{\boldsymbol{r}}_k) \quad (1)$$

where $\hat{\boldsymbol{r}}_j$ is the position of the jth particle and U is a short-range repulsive two-body interaction term. The quasicrystal potential is chosen to be eightfold rotation symmetric and centered on $\boldsymbol{r} = 0$,

$$V(\boldsymbol{r}) = V_0 \sum_{k=1}^{4} \cos^2(\mathbf{G}_k \cdot \boldsymbol{r}), \quad (2)$$

where V_0 is the potential amplitude and the quantities $\mathbf{G}_k$ are the lattice vectors of four mutually incoherent standing waves oriented at the angles 0°, 45°, 90°, and 135°, respectively. The lattice vectors have norm $|\mathbf{G}_k| = \pi/a$. We use the lattice spacing a and the corresponding recoil energy $E_r = \pi^2\hbar^2/2ma^2$ as the space and energy units, respectively [62]. The eightfold quasiperiodic potential, Eq. (2), has been recently realized for a system of ultracold bosons in Refs. [16,51].

The single-particle properties of the shallow 2D quasicrystal potential are qualitatively similar to its 1D counterpart (see, for instance, Refs. [29,79–81]). The critical localization potential V_c is found from accurate finite-size scaling analysis of the inverse participation ratio for the single-particle ground state (IPR_0), using exact diagonalization [62]. It shows a sharp transition between an extended phase for $V < V_c$ and a localized phase for $V > V_c$. Using square quasicrystal lattices of linear sizes up to $L = 128a$, we find $V_c/E_r \simeq 1.76 \pm 0.01$, which is in good agreement with the result of Ref. [63] found using another approach (ground-state curvature). Moreover, we find the critical behavior $\mathrm{IPR}_0 \sim (V - V_c)^\nu$ with the universal exponent $\nu \simeq 1/3$ [62].

We now turn to interacting bosons. In the low-energy s-wave scattering limit, the interaction potential $U(\boldsymbol{r})$ is fully characterized by the 2D scattering length a_{2D}. In practice, a quasi-2D Bose gas may be realized by strongly confining a 3D gas to zero point transverse oscillations. For a harmonic trap of angular frequency $\omega_\perp$, it requires that the excitation energy exceed the chemical potential μ and the temperature T, $\hbar\omega_\perp \gg \mu, k_B T$, with k_B the Boltzmann constant. The 2D scattering length is then determined by its 3D counterpart and the characteristic transverse length $l_\perp = \sqrt{\hbar/m\omega_\perp}$ [64,65],

$$a_{2D} \simeq 2.092 l_\perp \exp\left(-\sqrt{\frac{\pi}{2}} \frac{l_\perp}{a_{3D}} \right). \quad (3)$$

On the other hand, the interaction strength is characterized by the dimensionless mean field coupling constant $\tilde{g}$, such that the energy per particle in the homogenous gas is $E/N = \tilde{g} \times (\hbar^2 n/2m)$, with n the 2D density. In 2D, the quantity $\tilde{g}$ depends not only on a_{2D} but also on the chemical potential μ [57,64–66]. Up to logarithmic accuracy, it may be conveniently written [62]

$$\tilde{g} \simeq \frac{1}{\tilde{g}_0^{-1} + (4\pi)^{-1} \ln(\Lambda E_r/\mu)}, \quad (4)$$

where $\Lambda \simeq 0.141$ is a numerical constant and

$$\tilde{g}_0 = \frac{2\pi}{\ln(a/a_{2D})}. \quad (5)$$

The quantity $\tilde{g}_0$ is the relevant interaction parameter we shall use in the following.

Weak interactions.—We start with weakly interacting bosons, $\tilde{g} \ll 1$. In this regime, the phase diagram results from the competition of localization and interactions, and the superfluid fraction f_s may serve as an order parameter. While the quasicrystal potential tends to localize the bosons for $V > V_c$ and favor a BG phase ($f_s = 0$), the repulsive interactions tend to delocalize the bosons and restore superfluidity (SF, $f_s > 0$).

To determine the phase diagram, we first use a mean field approach. The ground-state dynamics of the Bose gas is then governed by the Gross-Pitaevskii equation (GPE):

$$\mu\psi = -\hbar^2\nabla^2\psi/2m + V(\boldsymbol{r})\psi + gN|\psi|^2\psi, \quad (6)$$

where $\psi(\boldsymbol{r})$ is the classical field and $g = (\hbar^2/m)\tilde{g}$ the dimensionful coupling constant, and we use the normalization condition $\int d\boldsymbol{r}|\psi(\boldsymbol{r})|^2 = 1$. Within the GPE, the mean field phase diagram is determined by only two universal dimensionless parameters, namely the potential amplitude V_0/E_r and the coupling coefficient gn/E_r. The field $\psi(\boldsymbol{r})$ is found using imaginary time evolution from an arbitrary state. It yields the total energy E and the chemical potential μ. The superfluid fraction is found from the boost approach using twisted boundary conditions,

$$f_s = \frac{2m}{\hbar^2 n} \lim_{\Theta\to 0} \frac{E_\Theta - E_0}{\Theta^2}, \quad (7)$$

where E_Θ is the energy for the phase difference Θ at opposite sides of the system [82,83].

Figure 1 is the phase diagram of the weakly interacting Bose gas against V_0/E_r and gn/E_r. It shows two distinct regimes, separated by a sharp line (see details below). For low interactions and/or a strong quasicrystal potential, the

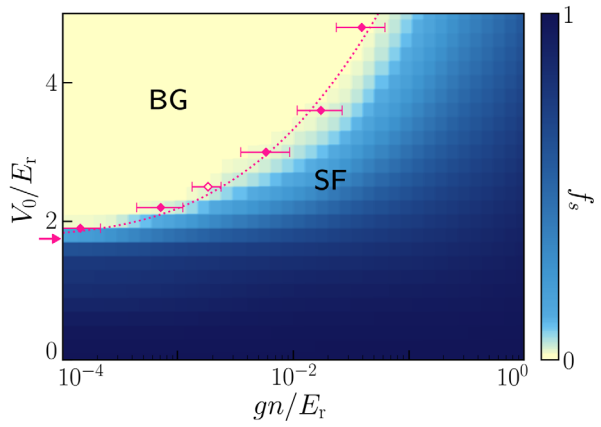

FIG. 1. Phase diagram of the weakly interacting Bose gas in a 2D quasicrystal lattice. The mean field SF fraction f_s is shown in color scale for a system of linear size $L = 20a$. It exhibits a BG phase ($f_s = 0$, yellow) and a SF phase ($f_s > 0$, blue), separated by a narrow intermediate region. The exact critical line is found from QMC calculations at $\tilde{g}_0 = 0.03$ (pink points; the dotted line is a guide to the eye). The hollow pink point corresponds to the transition found in Fig. 3. The pink arrow indicates the single-particle critical point $V_c \simeq 1.76E_r$.

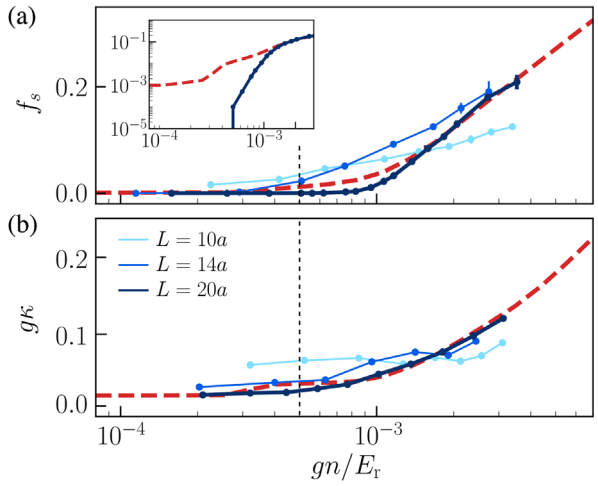

FIG. 2. Interaction-driven BG-SF transition for $V_0 = 2.2E_r$. (a) SF fraction (semi log scale), with magnification of the critical region in inset (log-log scale), and (b) compressibility (semi log scale). The dashed red lines show the mean field GPE results for a system size $L = 20a$. The blue points and solid lines show the QMC results for a fixed interaction parameter, $\tilde{g}_0 = 0.03$, and increasing system sizes $L/a = 10$, 14, 20 (from light to dark blue). The dashed black line indicates the BG-SF critical point.

mean field SF fraction vanishes and we find a BG phase (yellow region). Up to numerical accuracy, we find $f_s = 0$, except close to the separation line. For strong enough interactions and low quasiperiodic potential, we find $f_s > 0$, corresponding to the SF phase (blue region). For $V_0 < V_c$, there is no localization and the Bose gas is always in the SF phase, although with $f_s < 1$, except in the limit of a vanishing quasicrystal potential, $V_0 \to 0$. As expected, the SF-BG transition coincides with the single-particle localization point in the limit of vanishing interactions, $gn \to 0$ (pink arrow). Increasing repulsive interactions compete with localization induced by the quasicrystal potential and the critical point is shifted toward higher potential strengths. An analogous effect has also been observed in 1D interacting Fermi gases [84].

While these results are compatible with a SF-BG phase transition, the critical line is smoothed out by mean field effects [see Fig. 2(a) (dashed red line)]. To locate the transition line accurately, we now turn to *ab initio* quantum Monte Carlo (QMC) calculations. Our algorithm relies on the continuous space, path integral representation, simulating the exact Eq. (1) Hamiltonian. The QMC configurations are efficiently sampled using the worm algorithm within the grand canonical ensemble [85,86], and we use a generalized interaction propagator applicable to both weak and strong interactions [62]. We work at a vanishingly small temperature, $T = 0.0025E_r/k_B$ [87], and a fixed value of the interaction parameter, $\tilde{g}_0 = 0.03$. For such a small value, the μ-dependent term in Eq. (4) is negligible in our calculations and $\tilde{g} \simeq \tilde{g}_0 \ll 1$, corresponding to the weakly interacting regime. For each value of the potential amplitude V_0, we then scan the chemical potential μ and determine the density n from the statistics of the QMC world lines. The SF fraction is determined as $f_s = \Upsilon/n$, where the SF stiffness Υ is computed using the winding number estimator with periodic boundary conditions [88].

The QMC results for the SF fraction are plotted versus the mean field interaction parameter gn on Fig. 2(a) for increasing system sizes (corresponding to darker blue lines). For a large enough system, the QMC results fit well the mean field GPE prediction except in the critical region. While the GPE result is smooth, the QMC results show a sharp transition from the BG phase ($f_s = 0$) to the SF phase ($f_s > 0$) [see magnification in log-log scale in the inset of Fig. 2(a)]. Proceeding similarly for various amplitudes V_0 of the quasicrystal potential and still $\tilde{g}_0 = 0.03$, we determine the exact SF-BG critical line shown on Fig. 1 (see pink points; the dotted line is a guide to the eye). The QMC critical line fits well within the mean field crossover region. Hence, although criticality requires truly many-body effects, mean field calculations yield a reasonable estimate of the SF-BG transition.

We have also computed the compressibility $\kappa = \partial n/\partial\mu$ across the transition. Mean field and QMC results are plotted on Fig. 2(b), showing an excellent agreement for sufficiently large systems. In contrast to the SF fraction, the compressibility shows a smooth crossover from the BG phase to the SF phase, which is consistent with the expectation that both are compressible phases. More precisely, the compressibility is progressively suppressed by localization all the way from the SF limit to the BG limit with no signature of the critical point.

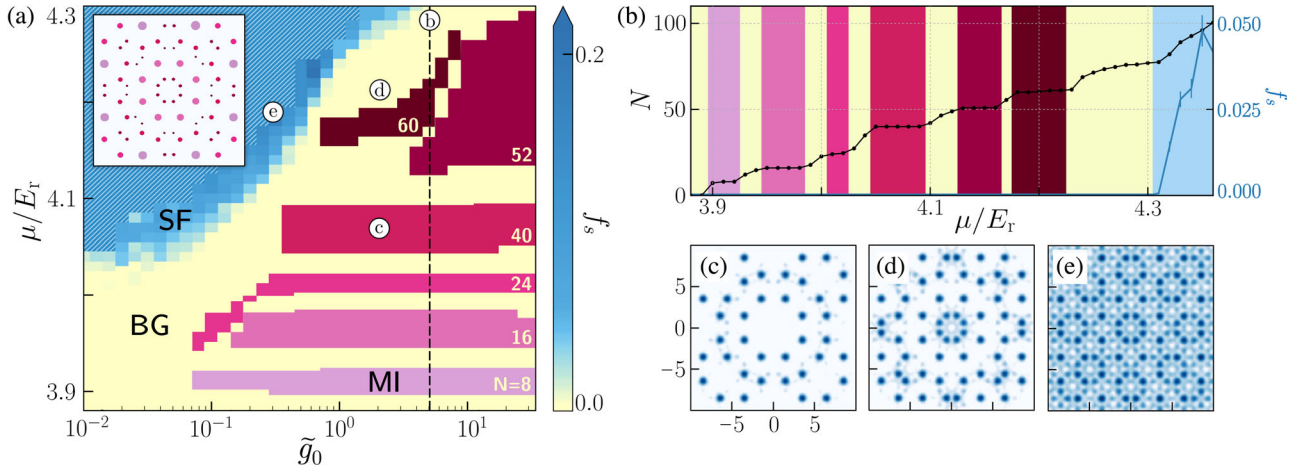

FIG. 3. (a) Phase diagram versus the interaction parameter $\tilde{g}_0$ and the chemical potential μ for $V_0 = 2.5E_r$ and a size $L = 20a$ as found using QMC calculations. The SF fraction f_s is shown in yellow-blue color scale. The purple-red regions indicate MI lobes with fillings $N = 8, 16, 24, 40, 52, 72$ (from lighter to darker), respectively. Inset: Filling of the potential wells for an increasing particle number. The inset shows a sketch of the potential wells, each colored according to the color of the MI lobe that fills it first. (b) Vertical cut in the phase diagram at $\tilde{g}_0 = 5$ (dashed black line), showing the number of particles N (black joint dots) and the superfluid fraction f_s (blue joint dots) against the chemical potential μ. (c)–(e) Density profiles in logarithmic color scale at the three points indicated on panel (a), in, respectively, the $N = 40$ MI, the BG, and the SF phases.

Strong interactions.—We now turn to strongly interacting bosons. In this case, the mean field GPE approach is no longer valid and we only rely on QMC calculations. We compute the superfluid fraction f_s and the compressibility κ as above, using the generalized interaction propagator [62]. Figure 3(a) shows the phase diagram against the interaction parameter $\tilde{g}_0$ and the chemical potential μ for the potential amplitude $V_0 = 2.5E_r > V_c$ and a square system of linear size $L = 20a$. For $\tilde{g}_0 \ll 1$, we recover the SF-BG phase transition discussed above. The critical point for $\tilde{g}_0 = 0.01$ is found at $\mu_c \simeq 4.03E_r$ and $gn_c \simeq 1.9 \times 10^{-3}E_r$ [see Fig. 3(a) and the hollow pink points on Fig. 1]. This behavior persists up to $\tilde{g}_0 \sim 0.06$. For stronger interactions, beyond mean field effects shift the critical point toward higher chemical potentials and, correspondingly, higher densities. Moreover, Mott lobes open (MI, purple-red regions). Figure 3(b) is a cut of the phase diagram at $\tilde{g}_0 = 5$ [see black dashed line on Fig. 3(a)]. It shows a clear SF transition from $f_s = 0$ to $f_s > 0$ at $\mu_c \simeq 4.31E_r$. In the insulating phase ($f_s = 0$), we find a series of Mott plateaus characterized by a vanishing compressibility, $\kappa = L^{-2}\partial N/\partial\mu = 0$. We have checked that, consistently, the fluctuations of the total number of particles N exactly vanishes. These Mott lobes emerge due to large repulsive interactions, which localize the particles in the deepest wells, thus forming an incompressible insulator with integer fillings. Because of the eightfold rotational symmetry of the quasicrystal potential, the total number of particles is usually a multiple of 8, namely $N = 8$, 16, 24, 40 [see numbers on Fig. 3(a)]. They progressively fill the lowest-energy potential wells, sketched with corresponding colors and decreasing sizes in the inset of Fig. 3(a).

Two exceptions are the $N = 52$ and $N = 60$ lobes. They feature 40 particles localized in the 40 deepest wells similar to the fourth lobe, plus additional particles in the next 24 wells. Among these wells, 16 come in 8 pairs of close-by wells, corresponding to the small dots on the very top center of the inset of Fig. 3(a) and those obtained by successive rotations of angle $\pi/4$. For the $N = 60$ lobe, all these sites are populated by a particle, while for the $N = 52$ lobe, only one of the partners of each pair is populated while the other one is empty. The remaining eight wells form the shortest eightfold ring in the center and one of every two wells contains a particle for both the $N = 52$ and $N = 60$ lobes. For each lobe, there are several configurations corresponding to the choice of the filled and empty sites, and we find that the QMC density profile randomly blinks between them all, hence spontaneously breaking the eightfold rotation symmetry. Similar symmetry breaking was previously found for long-range interactions [59]. Here, we quite unexpectedly find it for short-range interactions. We attribute this behavior to significant repulsion from the tails of the states bound in the nearest wells of the quasicrystal potential. Although their overlap is weak, strong-enough interactions prevent two particles from sitting even in different wells.

Figure 3(c)–(e) show the density profile for three selected points in the phase diagram [see Fig. 3(a)]. The first one corresponds to the $N = 40$ MI with exactly one particle in the 40 deepest wells. The second one corresponds to a BG. It features $N = 56$ particles in 56 distinct wells plus an incommensurate number of particles in the central eight wells. The latter form a small superfluid ring, which contributes a small finite compressibility but not global superfluidity. When the chemical potential increases

or the interactions decrease, such local superfluids proliferate and finally merge. The third density plot corresponds to a global SF with delocalized particles.

Conclusions.—We have determined the quantum phase diagram of weakly and strongly interacting 2D bosons in a shallow quasicrystal potential. The SF, BG, and MI quantum phases can be observed in current generation experiments with ultracold atoms using a combination of interference, spectroscopy, and transport measurements [46,48,51]. We have considered the same eightfold potential as in Refs. [16,51], but we expect our results to qualitatively hold also for other quasicrystalline potentials [15,38] as well as other configurations designed for photonic systems in the nonlinear regime [7]. Control of the 2D interaction in the range $0.05 \lesssim \tilde{g} \lesssim 3$ has been demonstrated in Ref. [67]. It is sufficient to observe the phase diagram of Fig. 3(a) and in particular the still elusive BG phase in 2D. Using sufficiently large samples in box-shaped traps could, for instance, yield further insight to the transitions discussed in this work, including critical exponents.

The use of shallow quasiperiodic potentials as considered in this Letter is promising for overcoming stringent temperature effects in the observation of the BG phase, as recently shown in 1D [29]. Yet, finite temperatures show richer behavior in 2D compared to 1D, in particular topological phase transitions. For instance, in a uniform 2D Bose gas, the SF-to-normal fluid transition is of the Berezinskii-Kosterlitz-Thouless type at some critical temperature [68,89–92]. While disorder with short-range correlations does not affect this transition [69,93], to our knowledge, the effect of long-range quasiperiodic order remains an open question.

We thank Markus Holzmann and Hélène Perrin for discussions about 2D scattering theory, and the CPHT computer team for valuable support. This research was supported by the Paris region DIM-SIRTEQ. The numerical calculations were performed using HPC resources from GENCI-CINES (Grant No. 2019-A0070510300) and make use of the ALPS scheduler library and statistical analysis tools [94–96].

[1] R. Penrose, The role of aesthetics in pure and applied mathematical research, Bull. Inst. Math. Appl. **10**, 266 (1974).
[2] B. Grùunbaum and G. C. Shepard, *Tilings and Patterns* (W. H. Freeman Publishers, San Francisco, 1987).
[3] M. Senechal, *Quasicrystals and Geometry* (Cambridge University Press, Cambridge, England, 1995).
[4] D. Shechtman, I. Blech, D. Gratias, and J. W. Cahn, Metallic Phase with Long-Range Orientational Order and No Translational Symmetry, Phys. Rev. Lett. **53**, 1951 (1984).
[5] W. Steurer, Twenty years of structure research on quasicrystals. Part I. Pentagonal, octagonal, decagonal and dodecagonal quasicrystals, Z. Kristallogr. Cryst. Mater. **219**, 391 (2004).
[6] W. Steurer, Quasicrystals: What do we know? What do we want to know? What can we know?, Acta Crystallogr. Sect. A **74**, 1 (2018).
[7] Z. V. Vardeny, A. Nahata, and A. Agrawal, Optics of photonic quasicrystals, Nat. Photonics **7**, 177 (2013).
[8] D. Tanese, E. Gurevich, F. Baboux, T. Jacqmin, A. Lemaître, E. Galopin, I. Sagnes, A. Amo, J. Bloch, and E. Akkermans, Fractal Energy Spectrum of a Polariton Gas in a Fibonacci Quasiperiodic Potential, Phys. Rev. Lett. **112**, 146404 (2014).
[9] F. Baboux, E. Levy, A. Lemaître, C. Gómez, E. Galopin, L. Le Gratiet, I. Sagnes, A. Amo, J. Bloch, and E. Akkermans, Measuring topological invariants from generalized edge states in polaritonic quasicrystals, Phys. Rev. B **95**, 161114 (2017).
[10] V. Goblot, A. Strkalj, N. Pernet, J. L. Lado, C. Dorow, A. Lemaître, L. L. Gratiet, A. Harouri, I. Sagnes, S. Ravets *et al.*, Emergence of criticality through a cascade of delocalization transitions in quasiperiodic chains, Nat. Phys. **16**, 832 (2020).
[11] L. Sanchez-Palencia and M. Lewenstein, Disordered quantum gases under control, Nat. Phys. **6**, 87 (2010).
[12] G. Modugno, Anderson localization in Bose-Einstein condensates, Rep. Prog. Phys. **73**, 102401 (2010).
[13] N. Macé, A. Jagannathan, and M. Duneau, Quantum simulation of a 2D quasicrystal with cold atoms, Crystals **6**, 124 (2016).
[14] D. Levine and P. J. Steinhardt, Quasicrystals: A New Class of Ordered Structures, Phys. Rev. Lett. **53**, 2477 (1984).
[15] L. Sanchez-Palencia and L. Santos, Bose-Einstein condensates in optical quasicrystal lattices, Phys. Rev. A **72**, 053607 (2005).
[16] K. Viebahn, M. Sbroscia, E. Carter, J.-C. Yu, and U. Schneider, Matter-Wave Diffraction from a Quasicrystalline Optical Lattice, Phys. Rev. Lett. **122**, 110404 (2019).
[17] L.-J. Lang, X. Cai, and S. Chen, Edge States and Topological Phases in One-Dimensional Optical Superlattices, Phys. Rev. Lett. **108**, 220401 (2012).
[18] Y. E. Kraus and O. Zilberberg, Topological Equivalence Between the Fibonacci Quasicrystal and the Harper Model, Phys. Rev. Lett. **109**, 116404 (2012).
[19] Y. E. Kraus, Z. Ringel, and O. Zilberberg, Four-Dimensional Quantum Hall Effect in a Two-Dimensional Quasicrystal, Phys. Rev. Lett. **111**, 226401 (2013).
[20] A. Dareau, E. Levy, M. B. Aguilera, R. Bouganne, E. Akkermans, F. Gerbier, and J. Beugnon, Revealing the Topology of Quasicrystals with a Diffraction Experiment, Phys. Rev. Lett. **119**, 215304 (2017).
[21] H. Huang and F. Liu, Quantum Spin Hall Effect and Spin Bott Index in a Quasicrystal Lattice, Phys. Rev. Lett. **121**, 126401 (2018).
[22] S. Aubry and G. André, Analyticity breaking and Anderson localization in incommensurate lattices, Ann. Isr. Phys. Soc. **3**, 133 (1980).
[23] G. Roati, C. D'Errico, L. Fallani, M. Fattori, C. Fort, M. Zaccanti, G. Modugno, M. Modugno, and M. Inguscio, Anderson localization of a non-interacting Bose-Einstein condensate, Nature (London) **453**, 895 (2008).

[24] B. Sutherland, Critical electronic wave functions on quasiperiodic lattices: Exact calculation of fractal measures, Phys. Rev. B **35**, 9529 (1987).
[25] H. Q. Yuan, U. Grimm, P. Repetowicz, and M. Schreiber, Energy spectra, wave functions, and quantum diffusion for quasiperiodic systems, Phys. Rev. B **62**, 15569 (2000).
[26] M. Kohmoto, Metal-Insulator Transition and Scaling for Incommensurate Systems, Phys. Rev. Lett. **51**, 1198 (1983).
[27] C. Tang and M. Kohmoto, Global scaling properties of the spectrum for a quasiperiodic Schrödinger equation, Phys. Rev. B **34**, 2041 (1986).
[28] T. S. Cubitt, D. Perez-Garcia, and M. M. Wolf, Undecidability of the spectral gap, Nature (London) **528**, 207 (2015).
[29] H. Yao, H. Khoudli, L. Bresque, and L. Sanchez-Palencia, Critical Behavior and Fractality in Shallow One-Dimensional Quasiperiodic Potentials, Phys. Rev. Lett. **123**, 070405 (2019).
[30] H. Yao, T. Giamarchi, and L. Sanchez-Palencia, Lieb-Liniger Bosons in a Shallow Quasiperiodic Potential: Bose Glass Phase and Fractal Mott Lobes, Phys. Rev. Lett. **125**, 060401 (2020).
[31] K. Kamiya, T. Takeuchi, N. Kabeya, N. Wada, T. Ishimasa, A. Ochiai, K. Deguchi, K. Imura, and N. Sato, Discovery of superconductivity in quasicrystal, Nat. Commun. **9**, 154 (2018).
[32] S. J. Ahn, P. Moon, T.-H. Kim, H.-W. Kim, H.-C. Shin, E. H. Kim, H. W. Cha, S.-J. Kahng, P. Kim, M. Koshino *et al.*, Dirac electrons in a dodecagonal graphene quasicrystal, Science **361**, 782 (2018).
[33] W. Yao, E. Wang, C. Bao, Y. Zhang, K. Zhang, K. Bao, C. K. Chan, C. Chen, J. Avila, M. C. Asensio *et al.*, Quasicrystalline 30° twisted bilayer graphene as an incommensurate superlattice with strong interlayer coupling, Proc. Natl. Acad. Sci. U.S.A. **115**, 6928 (2018).
[34] Y. S. Chan, C. T. Chan, and Z. Y. Liu, Photonic Band Gaps in Two Dimensional Photonic Quasicrystals, Phys. Rev. Lett. **80**, 956 (1998).
[35] Y. Lahini, R. Pugatch, F. Pozzi, M. Sorel, R. Morandotti, N. Davidson, and Y. Silberberg, Observation of a Localization Transition in Quasiperiodic Photonic Lattices, Phys. Rev. Lett. **103**, 013901 (2009).
[36] B. Freedman, G. Bartal, M. Segev, R. Lifshitz, D. N. Christodoulides, and J. W. Fleischer, Wave and defect dynamics in nonlinear photonic quasicrystals, Nature (London) **440**, 1166 (2006).
[37] Z. V. Vardeny, A. Nahata, and A. Agrawal, Optics of photonic quasicrystals, Nat. Photonics **7**, 177 (2013).
[38] L. Guidoni, C. Triché, P. Verkerk, and G. Grynberg, Quasiperiodic Optical Lattices, Phys. Rev. Lett. **79**, 3363 (1997).
[39] R. Roth and K. Burnett, Phase diagram of bosonic atoms in two-color superlattices, Phys. Rev. A **68**, 023604 (2003).
[40] B. Damski, J. Zakrzewski, L. Santos, P. Zoller, and M. Lewenstein, Atomic Bose and Anderson Glasses in Optical Lattices, Phys. Rev. Lett. **91**, 080403 (2003).
[41] T. Roscilde, Bosons in one-dimensional incommensurate superlattices, Phys. Rev. A **77**, 063605 (2008).
[42] G. Roux, T. Barthel, I. P. McCulloch, C. Kollath, U. Schollwöck, and T. Giamarchi, Quasiperiodic Bose-Hubbard model and localization in one-dimensional cold atomic gases, Phys. Rev. A **78**, 023628 (2008).
[43] B. Gadway, D. Pertot, J. Reeves, M. Vogt, and D. Schneble, Glassy Behavior in a Binary Atomic Mixture, Phys. Rev. Lett. **107**, 145306 (2011).
[44] A. Jagannathan and M. Duneau, An eightfold optical quasicrystal with cold atoms, Europhys. Lett. **104**, 66003 (2013).
[45] S. Lellouch and L. Sanchez-Palencia, Localization transition in weakly-interacting Bose superfluids in one-dimensional quasiperdiodic lattices, Phys. Rev. A **90**, 061602(R) (2014).
[46] C. D'Errico, E. Lucioni, L. Tanzi, L. Gori, G. Roux, I. P. McCulloch, T. Giamarchi, M. Inguscio, and G. Modugno, Observation of a Disordered Bosonic Insulator from Weak to Strong Interactions, Phys. Rev. Lett. **113**, 095301 (2014).
[47] M. Schreiber, S. S. Hodgman, P. Bordia, H. P. Lüschen, M. H. Fischer, R. Vosk, E. Altman, U. Schneider, and I. Bloch, Observation of many-body localization of interacting fermions in a quasi-random optical lattice, Science **349**, 842 (2015).
[48] L. Gori, T. Barthel, A. Kumar, E. Lucioni, L. Tanzi, M. Inguscio, G. Modugno, T. Giamarchi, C. D'Errico, and G. Roux, Finite-temperature effects on interacting bosonic one-dimensional systems in disordered lattices, Phys. Rev. A **93**, 033650 (2016).
[49] V. Khemani, D. N. Sheng, and D. A. Huse, Two Universality Classes for the Many-Body Localization Transition, Phys. Rev. Lett. **119**, 075702 (2017).
[50] T. Kohlert, S. Scherg, X. Li, H. P. Lüschen, S. Das Sarma, I. Bloch, and M. Aidelsburger, Observation of Many-Body Localization in a One-Dimensional System with a Single-Particle Mobility Edge, Phys. Rev. Lett. **122**, 170403 (2019).
[51] M. Sbroscia, K. Viebahn, E. Carter, J.-C. Yu, A. Gaunt, and U. Schneider, Observing Localization in a 2D Quasicrystalline Optical Lattice, Phys. Rev. Lett. **125**, 200604 (2020).
[52] F. A. An, K. Padavić, E. J. Meier, S. Hegde, S. Ganeshan, J. Pixley, S. Vishveshwara, and B. Gadway, Observation of tunable mobility edges in generalized Aubry-André lattices, arXiv:2007.01393.
[53] S. Gopalakrishnan, I. Martin, and E. A. Demler, Quantum Quasicrystals of Spin-Orbit-Coupled Dipolar Bosons, Phys. Rev. Lett. **111**, 185304 (2013).
[54] J. Hou, H. Hu, K. Sun, and C. Zhang, Superfluid-Quasicrystal in a Bose-Einstein Condensate, Phys. Rev. Lett. **120**, 060407 (2018).
[55] F. Mivehvar, H. Ritsch, and F. Piazza, Emergent Quasicrystalline Symmetry in Light-Induced Quantum Phase Transitions, Phys. Rev. Lett. **123**, 210604 (2019).
[56] M. Lewenstein, A. Sanpera, V. Ahufinger, B. Damski, A. Sen, and U. Sen, Ultracold atomic gases in optical lattices: Mimicking condensed matter physics and beyond, Adv. Phys. **56**, 243 (2007).
[57] I. Bloch, J. Dalibard, and W. Zwerger, Many-body physics with ultracold gases, Rev. Mod. Phys. **80**, 885 (2008).
[58] S. E. Pollack, D. Dries, M. Junker, Y. P. Chen, T. A. Corcovilos, and R. G. Hulet, Extreme Tunability of Interactions in a ^{7}Li Bose-Einstein Condensate, Phys. Rev. Lett. **102**, 090402 (2009).
[59] D. Johnstone, P. Öhberg, and C. W. Duncan, Mean-field phases of an ultracold gas in a quasicrystalline potential, Phys. Rev. A **100**, 053609 (2019).

[60] D. Johnstone, P. Öhberg, and C. W. Duncan, The Bose-glass phase in mean-field quasicrystalline systems, arXiv: 2008.08584.

[61] R. Ghadimi, T. Sugimoto, and T. Tohyama, Mean-field study of the Bose-Hubbard model in Penrose lattice, arXiv: 2005.04885.

[62] See Supplemental Material at http://link.aps.org/supplemental/10.1103/PhysRevLett.126.110401. It discusses the quasiperiodic potential and its single-particle localization properties, scattering theory in quasi-2D Bose gases, and the derivation of the 2D interaction propagator. It cites Refs. [29,30,51,57,63–78].

[63] A. Szabó and U. Schneider, Mixed spectra and partially extended states in a two-dimensional quasiperiodic model, Phys. Rev. B **101**, 014205 (2020).

[64] D. S. Petrov, M. Holzmann, and G. V. Shlyapnikov, Bose-Einstein Condensation in Quasi-2D Trapped Gases, Phys. Rev. Lett. **84**, 2551 (2000).

[65] D. Petrov and G. Shlyapnikov, Interatomic collisions in a tightly confined Bose gas, Phys. Rev. A **64**, 012706 (2001).

[66] L. Pricoupenko and M. Olshanii, Stability of two-dimensional Bose gases in the resonant regime, J. Phys. B **40**, 2065 (2007).

[67] L.-C. Ha, C.-L. Hung, X. Zhang, U. Eismann, S.-K. Tung, and C. Chin, Strongly Interacting Two-Dimensional Bose Gases, Phys. Rev. Lett. **110**, 145302 (2013).

[68] Z. Hadzibabic, P. Krüger, M. Cheneau, B. Battelier, and J. Dalibard, Berezinskii-Kosterlitz-Thouless crossover in a trapped atomic gas, Nature (London) **441**, 1118 (2006).

[69] G. Carleo, G. Boéris, M. Holzmann, and L. Sanchez-Palencia, Universal Superfluid Transition and Transport Properties of Two-Dimensional Dirty Bosons, Phys. Rev. Lett. **111**, 050406 (2013).

[70] X. Zhang, C.-L. Hung, S.-K. Tung, and C. Chin, Observation of quantum criticality with ultracold atoms in optical lattices, Science **335**, 1070 (2012).

[71] C. De Rossi, R. Dubessy, K. Merloti, M. d. G. de Herve, T. Badr, A. Perrin, L. Longchambon, and H. Perrin, Probing superfluidity in a quasi two-dimensional Bose gas through its local dynamics, New J. Phys. **18**, 062001 (2016).

[72] M. Schick, Two-dimensional system of hard-core bosons, Phys. Rev. A **3**, 1067 (1971).

[73] C. Mora and Y. Castin, Extension of Bogoliubov theory to quasicondensates, Phys. Rev. A **67**, 053615 (2003).

[74] Z. Hadzibabic and J. Dalibard, Two-dimensional Bose fluids: An atomic physics perspective, Riv. Nuovo Cimento **34**, 389 (2011).

[75] D. S. Petrov, G. V. Shlyapnikov, and J. T. M. Walraven, Regimes of Quantum Degeneracy in Trapped 1D Gases, Phys. Rev. Lett. **85**, 3745 (2000).

[76] Y. Yan and D. Blume, Incorporating exact two-body propagators for zero-range interactions into n-body Monte Carlo simulations, Phys. Rev. A **91**, 043607 (2015).

[77] N. Khuri, A. Martin, J.-M. Richard, and T. T. Wu, Low-energy potential scattering in two and three dimensions, J. Math. Phys. (N.Y.) **50**, 072105 (2009).

[78] T. M. Whitehead, L. M. Schonenberg, N. Kongsuwan, R. J. Needs, and G. J. Conduit, Pseudopotential for the two-dimensional contact interaction, Phys. Rev. A **93**, 042702 (2016).

[79] D. J. Boers, B. Goedeke, D. Hinrichs, and M. Holthaus, Mobility edges in bichromatic optical lattices, Phys. Rev. A **75**, 063404 (2007).

[80] J. Biddle, B. Wang, D. J. Priour. Jr., and S. Das Sarma, Localization in one-dimensional incommensurate lattices beyond the Aubry-André model, Phys. Rev. A **80**, 021603 (2009).

[81] J. Biddle and S. Das Sarma, Predicted Mobility Edges in One-Dimensional Incommensurate Optical Lattices: An Exactly Solvable Model of Anderson Localization, Phys. Rev. Lett. **104**, 070601 (2010).

[82] M. E. Fisher, M. N. Barber, and D. Jasnow, Helicity modulus, superfluidity, and scaling in isotropic systems, Phys. Rev. A **8**, 1111 (1973).

[83] W. Krauth, N. Trivedi, and D. Ceperley, Superfluid-Insulator Transition in Disordered Boson Systems, Phys. Rev. Lett. **67**, 2307 (1991).

[84] S. Pilati and V. K. Varma, Localization of interacting Fermi gases in quasiperiodic potentials, Phys. Rev. A **95**, 013613 (2017).

[85] M. Boninsegni, N. Prokof'ev, and B. Svistunov, Worm Algorithm for Continuous-Space Path Integral Monte Carlo Simulations, Phys. Rev. Lett. **96**, 070601 (2006).

[86] M. Boninsegni, N. V. Prokof'ev, and B. V. Svistunov, Worm algorithm and diagrammatic Monte Carlo: A new approach to continuous-space path integral Monte Carlo simulations, Phys. Rev. E **74**, 036701 (2006).

[87] This temperature is much smaller than any relevant temperature scale in the calculations. Moreover, we have checked that further decreasing the temperature does not significantly alter the results.

[88] D. M. Ceperley, Path integrals in the theory of condensed helium, Rev. Mod. Phys. **67**, 279 (1995).

[89] V. L. Berezinskii, Destruction of long-range order in one-dimensional and two-dimensional systems possessing a continuous symmetry group. II. Quantum systems, Sov. Phys. JETP **34**, 610 (1972).

[90] J. M. Kosterlitz and D. J. Thouless, Ordering, metastability and phase transitions in two-dimensional systems, J. Phys. C **6**, 1181 (1973).

[91] R. Desbuquois, L. Chomaz, T. Yefsah, J. Léonard, J. Beugnon, C. Weitenberg, and J. Dalibard, Superfluid behaviour of a two-dimensional Bose gases, Nat. Phys. **8**, 645 (2012).

[92] T. Plisson, B. Allard, M. Holzmann, G. Salomon, A. Aspect, P. Bouyer, and T. Bourdel, Coherence properties of a two-dimensional trapped Bose gas around the superfluid transition, Phys. Rev. A **84**, 061606 (2011).

[93] A. Harris, Effect of random defects on the critical behaviour of Ising models, J. Phys. C **7**, 1671 (1974).

[94] M. Troyer, B. Ammon, and E. Heeb, Parallel object oriented Monte Carlo simulations, Lect. Notes Comput. Sci. **1505**, 191 (1998).

[95] A. Albuquerque, F. Alet, P. Corboz, P. Dayal, A. Feiguin, S. Fuchs, L. Gamper, E. Gull, S. Guertler, A. Honecker *et al.*, The ALPS project release 1.3: Open-source software for strongly correlated systems, J. Magn. Magn. Mater. **310**, 1187 (2007).

[96] B. Bauer, L. D. Carr, H. Evertz, A. Feiguin, J. Freire, S. Fuchs, L. Gamper, J. Gukelberger, E. Gull, S. Guertler *et al.*, The ALPS project release 2.0: Open source software for strongly correlated systems, J. Stat. Mech. (2011) P05001.